NANO LETTERS

2007
Vol. 7, No. 8
2513−2520

Real-Time Imaging of Astrocyte Response to Quantum Dots: In Vivo Screening Model System for Biocompatibility of Nanoparticles

Dusica Maysinger,*,† Maik Behrendt, Mélanie Lalancette-Hébert, and Jasna Kriz*,‡

Department of Pharmacology and Therapeutics, McGill University, Montreal, Quebec, Canada, and Department of Anatomy and Physiology, Centre de Recherche du CHUL, Faculty of Medicine, Laval University, Quebec, QC, Canada

Received July 4, 2007

ABSTRACT

Astrocytes are the principle macroglial brain cells. They are activated by different stressors and brain injuries. Quantum dots (QDs) can cause oxidative stress. This study shows a real-time imaging of primary cortical cultures and assessment of QD-induced activation of astrocytes in the brains of transgenic mice with the luciferase gene driven by the murine astrocyte promoter. This approach may be widely applicable for assessing the astroglia/tissue response to nanoparticles in live animals.

Different types of fluorescent nanoparticles were thoroughly characterized in cell lines, but very few were tested in primary cultures and live animals.

A number of laboratories, including ours, have explored the physicochemical properties of nanoparticles as drug delivery systems and as bioimaging tools.[1−4] Imaging of the whole animal using fluorescent micelles remains difficult because of limited micelle stability in complex biological media[5−6] and strong autofluorescence of tissues due to endogenous chromophores (e.g., collagens, porphyrins, and flavins). A new class of semiconductor-based nanoparticles (i.e., quantum dots) has recently emerged as a complementary imaging tool with superior photophysical properties, which can at least in part overcome the limitations of fluorescent dyes.[2,7,8] A broad range of nanoparticles were investigated in different cell lines in vitro.[7−10] A common observation in these studies was that reactive oxygen species (ROS) are formed. The consequences of ROS formation are different depending on the cell type, concentration, and duration of exposure to the QDs as well as several physical and chemical properties of nanoparticles.[11−15] Surface-modified quantum dots (QDs) with polyethylene glycol (PEG) were reported to be biocompatible in vitro.[16] The physical, chemical, and biological properties and availability of polyethylene glycol (PEG) made this polymer an attractive corona-forming candidate for micelles and quantum dots.[17−20] Micelles with PEG corona were studied quite extensively and PEG-QDs, e.g., QD 545 (green), QD 655 (orange), QD 705 (far red), and QD 805 (near infrared) are now commercially available and some of them have already been tested in vitro in keratinocytes,[16] but none have been used for real-time imaging in vivo. There are few reports on the distribution and pharmacokinetic properties[21−24] of other types of QDs. These studies show that cadmium selenide QDs are sequestered in several organs after iv administration[22] including lymph nodes[25] and solid tumors.[17]

The biocompatibility of intraparenchymaly administered QDs in live animals, especially after repeated imaging sessions, has not yet been reported. Approaches for an early and sensitive detection of glia and neuron responsiveness to nanoparticles or other nanomaterials are therefore needed. Astrocytes are the principle macroglial cell type in the brain and their activation is one of the key components of the cellular responses to stress and brain injuries. The passage from the quiescent to reactive astrocytes is associated with strong upregulation of the intermediate filament, glial fibrillary acidic protein (GFAP) in glia.[26,27] GFAP upregulation is considered a surrogate marker of neuronal stress and brain inflammatory response. Current methods of astrocyte and microglia detection are mainly based on immunocytochemistry. However, in recent years, imaging strategies employing

* Corresponding authors. E-mail: dusica.maysinger@mcgill.ca (D.M.); Jasna.Kriz@crchul.ulaval.ca (J.K.). Telephone: (514) 398-4400 x0838 (D.M.); Telephone: (418) 654-2296 (J.K.). Fax: (514) 398-6690 (D.M.); Fax: (418) 654-2761 (J.K.).

† Department of Pharmacology and Therapeutics, Faculty of Medicine, McGill University, 3655 Promenade Sir-William-Osler, Room 1314, McIntyre Medical Science Building, Montreal, Quebec, Canada H3G 1Y6.

‡ Department of Anatomy and Physiology, Centre de recherche du CHUL, Faculty of Medicine, Laval University, Quebec, QC, Canada, G1V 4G2.

10.1021/nl071611t CCC: $37.00
Published on Web 07/19/2007

Table 1. Some Photophysical Properties of Nanoparticels and Conditions for In Vivo Imaging in Real Time

nanoparticle core metals	cerium(IV) oxide CeO_2	QD non-PEG CdTe or CdSe	QD-PEG CdSe/ZnS
		nanoparticle sizes	
core diameter (nm)		~3−5	~3−8
particle diameter (nm)	≤7	~3−5	~20−50
		optimal conditions for FACS analysis	
excitation (nm)	nonfluorescent	**488**: QD 545, QD 565, QD 595, QD 655 **655**: QD 705	**488**: QD 545, QD 565, QD 595, QD 655 **655**: QD 705
filter sets	nonfluorescent	530/30: green 610/20: orange 695/40: far red	530/30: green 610/20: orange 695/40: far red
		optimal conditions for in vivo imaging	
excitation (nm)	nonfluorescent	400−450: QD 565 500−550: QD 655 615−665: QD 705	400−450: QD 565 500−550: QD 655 615−665: QD 705
filter sets	nonfluorescent	GFP: green DsRed: orange Cy5: far red	GFP : green DsRed: orange Cy5: far red
application in vivo	nonsuitable	nonsuitable (faint, transient signal	suitable (strong, lasting signal)

reporter molecules have been developed to study biological processes as they occur in living animals or cell assays. In our experiments, we took the advantage of transgenic mice that carry the luciferase gene under the transcriptional control of the murine GFAP promoter.[28] In this mouse model, upregulation of GFAP or luciferase expression in response to different stimuli (brain injection of QDs) can be analyzed noninvasively in living animals using biophotonic imaging and a high-resolution CCD camera.[29]

The objective of the present study was to explore the applicability of several PEGylated QDs in primary neural cultures and in the whole animals. We show a new approach for testing the biocompatibility of nanoparticles in vivo by employing luciferase-expressing transgenic mice, driven by an astrocyte-specific promoter, as a sensitive reporter system of astrocyte activation by nanoparticles.

Experiments in these studies were designed with the following aims: (i) to compare the suitability of several commercial QDs for imaging live cells and mice, (ii) to examine if repeated exposure to laser light causes marked cell damage or glial activation at the site or in the proximity of QD administration in the brain, and (iii) to assess subcellular localization of QDs in the mouse primary cortical cultures.

Properties of Selected Nanoparticles. To assess the suitability of nanoparticles for imaging in cell cultures and in vivo we used several types of QDs (commercial PEGylated QD 545, QD 655, QD 705, and noncommercial non-PEGylated CdTe QDs) and cerium oxide.

Characteristic physical and morphological properties of these nanoparticles were reported,[5,6,16,30] and some of them pertinent to this study are summarized in Table 1. Although the QD core compositions (CdTe and CdSe) were different, emission maxima for these types of nanoparticles were similar within the green and red spectra, respectively. The strongest fluorescence intensity was obtained from far-red-emitting PEGylated QDs 705 (705 ± 4 nm; median fluorescence intensity, MFI % > 2600), and the weakest relative fluorescent intensities were recorded from equimolar (30 nM) concentrations of PEGylated and non-PEGylated QDs emitting between 518 and 596 nm (MFI % < 100).

Uptake and Biocompatibility of QDs. To determine the extent of uptake of non-PEGylated and PEGylated fluorescent QDs, PC12 cells and primary cortical cultures were treated with these nanoparticles for 24 h (see Supporting Information Materials and Methods). Subsequently, spectrofluorometric analysis and fluorescent activated cell sorting (FACS) (PC12 cells) or confocal microscopy (primary cultures) was performed. There was barely any detectable signal from green non-PEGylated cadmium telluride QD 595 (MFI (%) = 98.75 ± 1.8; Figure 1A) and PEGylated QDs 545 MFI (%) = 96.25 ± 5.3). In contrast, a strong signal was measured in cells exposed to equivalent nanomolar concentrations (30 nM) of PEGylated QD 705 (MFI (%) = 2660 ± 208.6; Figure 1A).

In primary neural cultures, the uptake of all QDs varied markedly with the relative ratios between glia and neurons, but it was always consistently and significantly higher in glia than in neurons (<0.5% in neurons relative to glia). We therefore explored their subcellular distribution in glial cells as well as biological response of these cells in vivo (see section In Vivo Imaging of Intracortically Administered QD 705).

To reveal possible damaging effects of QDs at the cellular level, we used PC12 cells and cortical primary cultures (Figure 1B). The biocompatibility of QDs as assessed by a biochemical assay (Alamar blue) and confirmed by cell counting was not significantly different from naïve control PC12 cells, except when the cells were treated with non-PEGylated QD 595 (30nM; Figure 1B; bar QD 595, p <

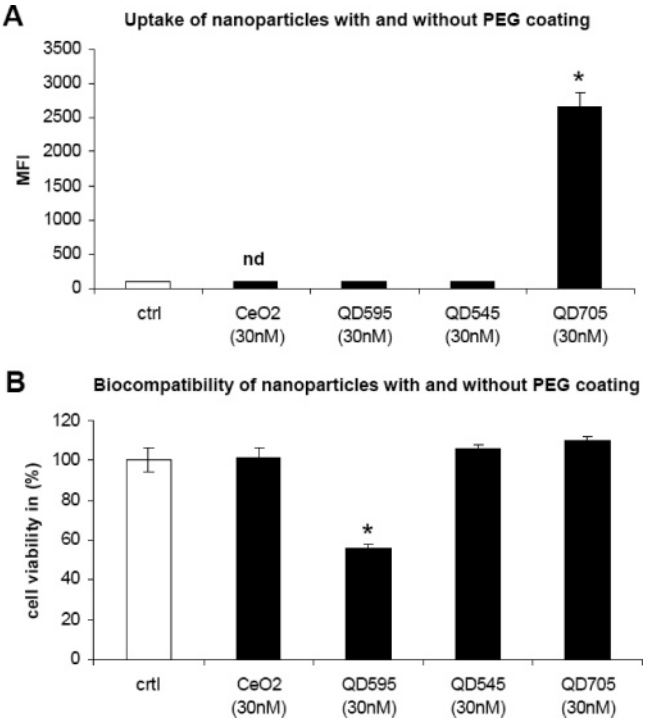

Figure 1. Uptake and biocompatibility of PEGylated and non-PEGylated nanoparticles. All experiments were carried out with rat pheochromocytoma cells (PC12) in cell cultures. All determinations were done after 24 h of exposure to nanoparticles in comparable concentrations. Panel A shows uptake determined by FACS and Panel B shows cell viability in the presence of the various QDs and cerium oxide for comparison. Cell viability in the presence of QDs was assessed by Alamar blue assay. Each bar represents the mean ± SEM (n = 3−5) from at least two independent experiments; nd = not detectable; differences were considered significant when $p < 0.05$.

0.05). These green, non-PEGylated QDs (in serum-free medium) caused almost 50% cell death (cell viability (%) = 56.03% ± 2.13). In contrast, treatment with cerium oxide nanoparticles (30 nM, equimolar to the QD) did not cause significant cell loss (cell viability (%) = 101.3% ± 5.28).

In Vivo Imaging of Locally Administered (sc) Different QDs. Having seen no extensive damage by the PEGylated QDs in cell cultures (Figure 1), we then assessed the intensity and duration of the fluorescence of the locally (subcutaneously, sc) administered QDs in live animals (Figure 2).

In the first study, 50 μL of QD 565 was injected in the lower back region of FVB/N mouse and imaged for fluorescence (Figure 2A).

The images show QD fluorescence from the same mouse at day 1 and day 7. QD concentrations, excitation, and filter settings for these studies are summarized in Supporting Information Tables S1, S2, and S3 together with the corresponding total photon flux (fluorescence intensity, TF) following 1 s imaging time. Green QDs were detected only initially but not after 7 days, whereas both orange and red QDs were still detectable. The results point toward the suitability of QD 705 for subcutaneous injections and support earlier findings obtained with different types of QDs.[16] QDs 705 were therefore used for real-time imaging after intracortical injections in the mouse brain.

In Vivo Imaging of Intracortically Administered QD 705. We explored whether PEGylated QD 705 can be visible in brain structures (i.e., cerebral cortex), which are much less accessible and difficult to image due to the protection by the skull. The results from these studies are illustrated in Figure 3 (panels A−T), and they show that 2.0 μL (16 pmoles) of QD 705 injected in the brain cortex can be detected immediately as well as at 1 h, 24 h, 72 h and 7 days postinjection (Figure 3, panels E −H). Although there was a time-dependent decline in the total photon fluxes, the photon emission from the intracerebrally injected QDs was quite stable and it was easily detectable 7 days after injection (Figure 3, panels E−H).

To verify whether microinjection of QDs in the brain cortex is associated with the induction of neighboring tissue inflammatory response and/or tissue damage, we employed the GFAP-luc (luciferase) transgenic mice. In this mouse model, the luciferase gene is expressed under the transcriptional control of the murine glial fibrilary acidic protein (GFAP) promoter,[28] therefore astrocyte activation (as a marker of inflammatory response) can be analyzed noninvasively and in living animals using bioluminescent imaging and a high-resolution CCD camera (IVIS 200 imaging system, Xenogen-Caliper LS, Alameda CA). In vivo light production reveals the spatial and temporal expression of the selected gene promoters in the living mice. As demonstrated in Figure 3 (panels I−L), the intracerebral injection of QDs 705 was associated with transient increase in GFAP signals/photon emission reaching the maximum 24 h after injection. The signal intensity was higher in animals receiving QD 705 as compared to control animals receiving the same volume of saline (Table 2). Interestingly, astrocyte activation was rather transient, as there was no marked difference in GFAP signals/photon emission between QD 705 and saline in mice 7 days after injection (Figure 3, panels L and D). To further validate our in vivo model system, we tested other nanoparticles whose properties were reported,[30,31] but their ability to induce an inflammatory response in the CNS was unknown. Nanoparticles selected for this purpose were: non-PEGylated cadmium telluride (CdTe) nanoparticles (Figure 3, panels Q−T), known to have cytotoxic properties,[31] and cerium oxide (CeO_2) nanoparticles, which have been shown to confer cell protection[14] (Figure 3, panels M−P). We used them as additional controls to longitudinally analyze astrocyte activation in GFAP-luc mice. The results from our studies demonstrated that intracerebral injection of CdTe QDs was indeed associated with a robust activation of astrocytes as revealed by a marked increase in bioluminescence that persisted for a week. The increase in GFAP signals induced by CdTe QDs was markedly higher than those by QD 705. In addition, there was a different temporal dynamics for these types of QDs; the peak was reached at day 3 (Figure 3, panels S and K) and CdTe-induced astrocyte activation still persisted at day 7 (Figure 3, panel T, Table 2; Figure S1, Supporting Information). In contrast to a strong tissue reaction to CdTe QDs, the injection of nontoxic CeO_2 nanoparticles showed a pattern of GFAP-signal induction similar to that of the saline (Figure 3, panels M−P and A−D, Table 2; Figure

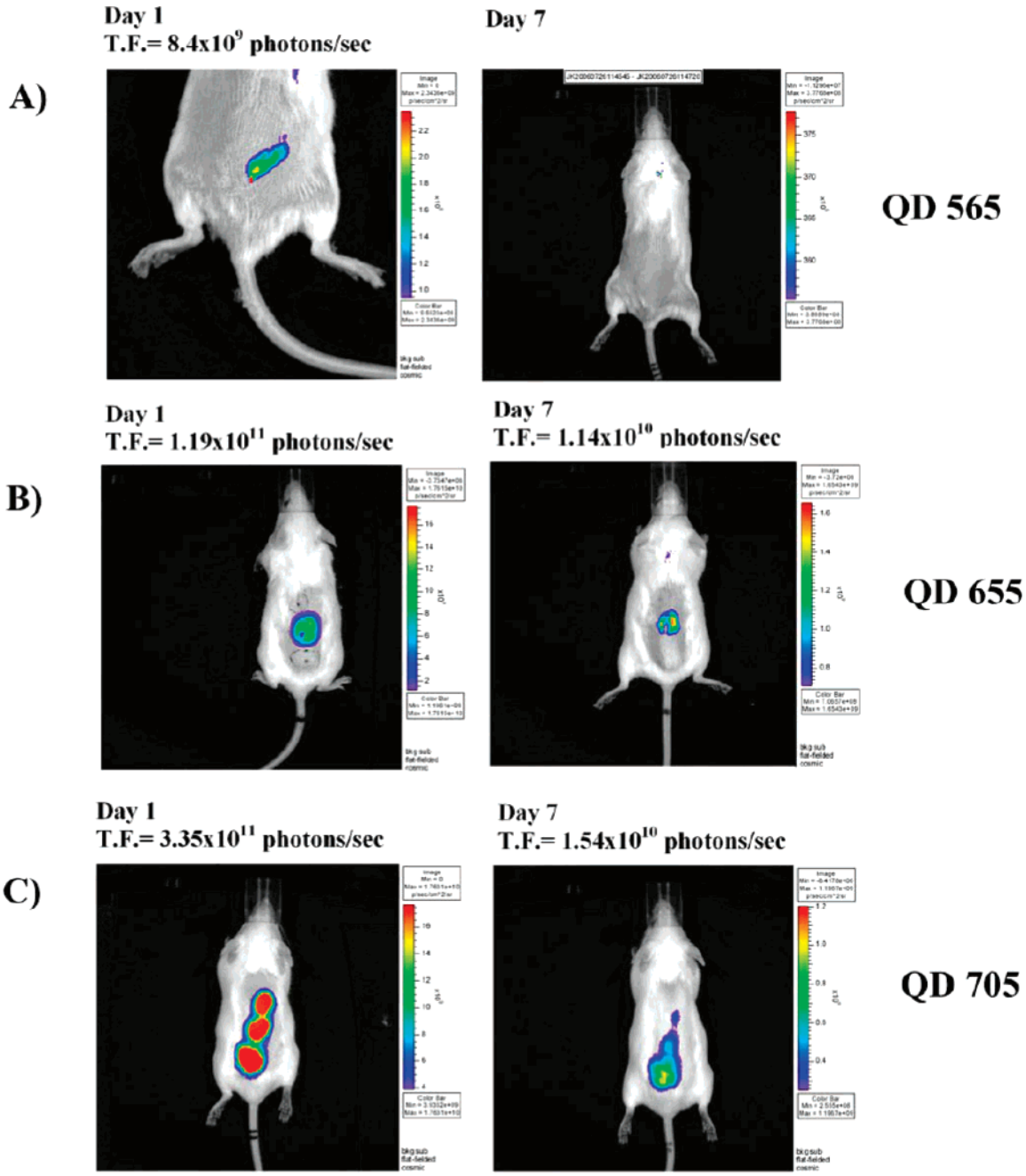

Figure 2. In vivo fluorescence imaging of subcutaneously injected QDs. Two to three month old FVB/N mice were injected subcutaneously with 10−50 μL of QDs. Pseudocolor fluorescence images of 50 μL of QD 565 (8 μM) (A), 50 μL of QD 655 (8 μM) (B), and 10 μL, 25 μL, and 50 μL of QD 705 (2.67 μM; 1:3 dilution in saline) (C) were acquired immediately and 7 days after subcutaneous QD injection using green, red-orange and far-red filter sets, respectively (Table 1). Fluorescence images were acquired with a 1 s exposure time for QD 565 and 0.5 s exposure time for QDs 655 and QDs 705, respectively. Total photon fluxes (TF) were determined at day 1 and 7 using region-of-interest (ROI) measurement and expressed in photons/s. The scales on the right are the color maps for photon counts.

S1, Supporting Information). The results from our study suggest that this in vivo mouse model can be applied for the screening of nanoparticle-induced glial activation, which can promote both cell survival and cell death in the brain. Quantitative data on signal intensities of astrocyte response from in vivo imaging on days 1, 2, 3, and 7 for QD 705, CeO_2 nanoparticles, and CdTe QDs are summarized in Table 2.

Because CeO_2 nanoparticles are nonfluorescent, the intracortical signal could not be obtained. Similarly, the signal intensity of fluorescent non-PEGylated CdTe QDs (2 uL, equivalent concentration to ceria and QD 705) was too weak and could not be detected. One possible explanation for the loss of fluorescence could be the interaction with tissue proteins resulting in quenching. Alternatively, CdTe unprotected QDs are unstable. It was recently shown that small, green QDs are rapidly taken up by stem cells and then eliminated,[14] providing an additional explanation for the loss of fluorescence. It is conceivable that these events are taking place under the conditions employed in the present study.

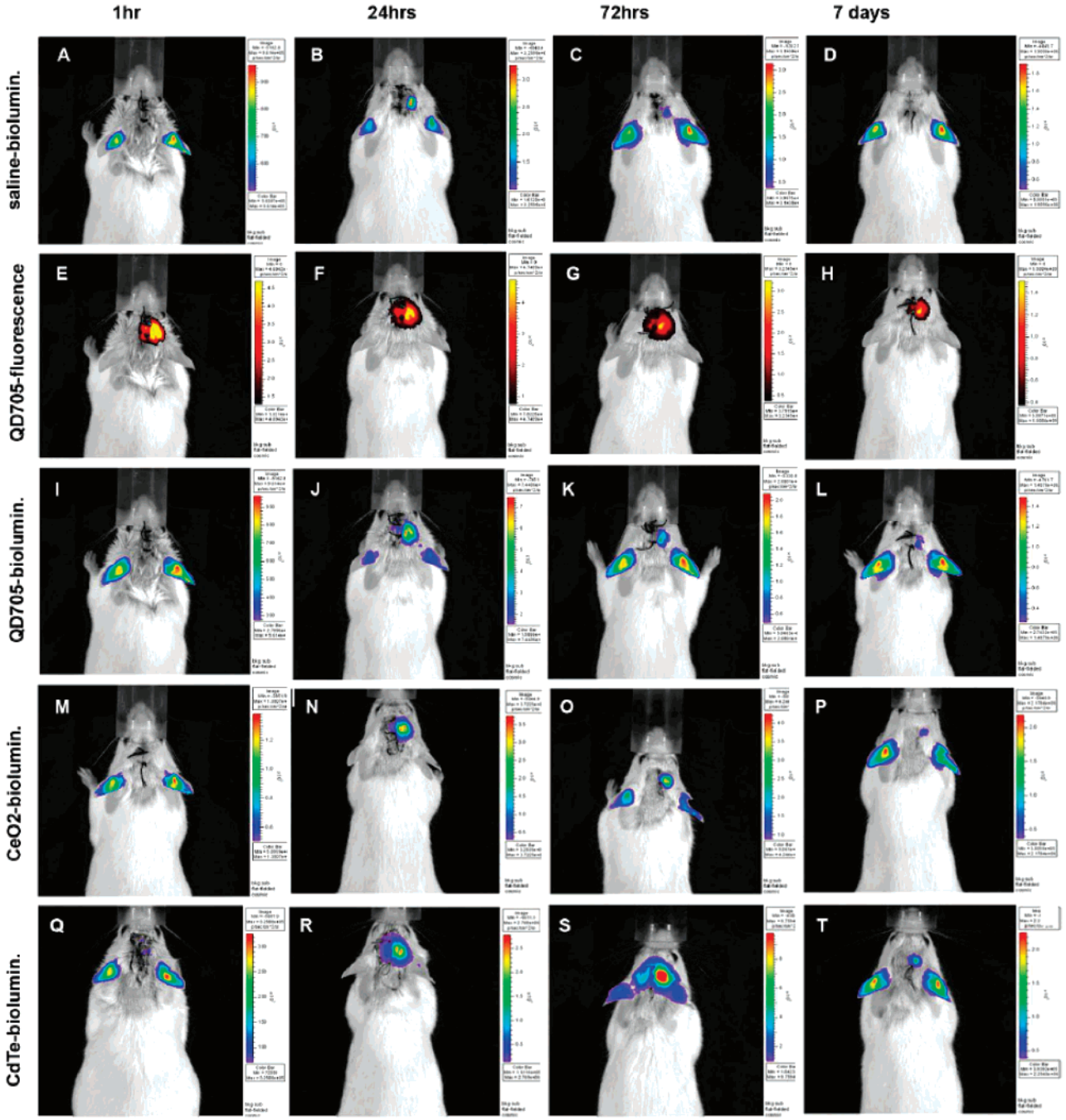

Figure 3. In vivo fluorescence and bioluminescence imaging of the brain reveals a robust increase in astrocyte response to CdTe QDs as compared to other tested nanoparticles. Representative pseudocolor fluorescence and bioluminescence images of PEGylated QD 705, CeO_2, non-PEGylated CdTe, and saline (control) stereotaxically injected in the right parietal cortex of the GFAP-luc reporter mouse (the coordinates for injection were: 2 mm posterior to bregma, 2 mm lateral to the midline, and 1.5 mm below the surface of the skull). The images were acquired using the far-red Filter set at 0.5 s exposure time for QD 705. Astrocyte activation was evaluated from the same mouse using in vivo bioluminescence. GFAP-luc mice were injected with luciferine (i.p. 150 mg/kg) prior to imaging bioluminescent signals. Total photon fluxes (TF) were determined at different postinjection time periods during 7 days and expressed in photons/s. Real-time visualization of bioluminescent GFAP-luciferase signals after intracerebral injection of saline is shown in panels (A−D) and those of in vivo fluorescence of intracortically injected QD 705 in panels (E−H). Bioluminescent imaging of QD 705 is shown in panels (I−L). Additional biocompatibility screening was performed for CeO_2 (M−-P) and non-PEGylated CdTe nanoparticles (Q−T). The images were longitudinally recorded from the same experimental animals within 7 days, revealing the dynamics of astrocyte activation throughout this observation time. The scales on the right are the color maps for photon counts, red indicating high and blue indicating low photons/s. Biolumienscent signals detected from the ears represent constitutively expressed GFAP in the subset of cartilage cells and were excluded from photon emission region of interest (ROI) analysis.

We therefore explored the site of QD 705 intracellular location 7 days after intracortical injection in vivo. The mice were killed by an overdose of anesthetic and perfused using 4% paraformaldehyde pH = 7.4. The brains were cut in 25 μm sections and blocked in TBS containing 5% goat serum and 0.20% Triton X-100 for 30 min. Using the same buffer

Table 2. Intensities of GFAP Signals in Astrocytes Activated by Intracortical Administration of Nanoparticles[a]

	saline	QD 705	CeO_2	CdTe
1 h	nd	nd	nd	nd
24 h	6.38×10^6 p/s	2.12×10^7 p/s	7.03×10^6 p/s	6.8×10^6 p/s
72 h	2.15×10^6 p/s	3.5×10^6 p/s	1.6×10^6 p/s	$\mathbf{5.34 \times 10^7}$ **p/s**
7 days	4.6×10^4 p/s	1.4×10^6 p/s	1.4×10^5 p/s	$\mathbf{2.8 \times 10^6}$ **p/s**

[a] Total photon fluxes (1 min bioluminescence imaging) are expressed in photons/s (p/s) and obtained from the brains of living mice after in vivo imaging. The values represent the intensity of GFAP of brain tissue reaction to different nanoparticle injections. nd = nondetectable.

solution, the sections were then incubated overnight at room temperature in primary antibody mouse monoclonal anti-GFAP (Sigma, Oakville, ON, Canada) and rabbit polyclonal anti-Iba1 (Wako, Richmond, VA) for detection of microglial cells. As expected from in vivo imaging data (Figure 3), the injection of QDs was associated with an increase in GFAP immunoreactivity and astrocyte activation (Figure 4, panels B and C), as well as activation of microglial cells (Figure 4, panels E and F).

The majority of injected QDs were localized within the Iba-1 positive microglial cells, which normally function as the brain phagocytes. Because inflammatory processes in the brain comprise microglial and astrocyte activation, both glial cell types can be used as markers for neuroinflammation.

Consistent with in vivo results, we further investigated the site of QD location in primary neural cortical cultures using the dual staining protocol. Mixed cortical cultures from 5 day old mice were used after one week in culture, and the exposure to QDs was for 4 h (Figure 5). During this time, there was no detectable damage to either neurons or glia. Dual labeling of live cells using MitoTracker (Figure 5B) and LysoTracker (Figure 5E) clearly revealed both organelles and QDs (Figure 5, panels A and D). All mitochondria were consistently green and elongated (Figure 5B). QDs 705 were dispersed between the mitochondria and there were no signal overlaps between the green and red, suggesting an absence of these nanoparticles within mitochondria. (Figure 5C). Green LysoTracker in the presence of red QDs yielded intensely yellow lysosomes suggesting their co-localization (Figure 5F). Similar results were obtained with PC12 cells (not shown), confirming the absence of co-localization between QD 705 and the mitochondrial marker. On the basis of the distinct morphological characteristics of glia and neurons, it was clear that, after 4 h of incubation, QDs 705 did not accumulate in cortical neurons, whereas glia contained significant amounts.

Results from these studies provide the first evidence for transient astrocyte activation in the cerebral cortex in live animals with locally injected PEGylated QDs and the robust neuroinflammatory response following non-PEGylated CdTe injection. The data suggest that PEGylated QD 705, followed by QDs 655 and 565 and ceria, are biocompatible in low nanomolar concentrations in primary neural cortical cultures and PC12 cells. Fluorescent activated cell sorting (FACS) and confocal microscopy showed that internalized QDs do not cause marked cell damage within one week and that PEGylated QDs accumulate in lysosomes of glial cells.

Engineered nanoparticles have been previously used for imaging of single cells, individual molecules, and whole animals.[21,22] In this study, we show real-time imaging for a week. In our live imaging experiments using sc injected PEGylated QDs 565, 655, and 705, we did not observe any marked cell damage or toxicity induced by multiple QD excitation during the 7 day period. These results are in accordance with previous observation showing that PEGylated QDs are biocompatible in human epithelial keratinocytes.[16] In contrast, the injection of QD 705 in the brain was associated with transient increase in the brain inflammatory response, as revealed by astrocyte activation and increase in GFAP signal (Figures 3 and 4). However, this early stimulation of astrocyte activation was transient, and by day 7, there was no marked difference between luciferase signal/photon emission around the injection site between QD treated and saline-injected control animals. These data suggest that PEGylated nanoparticles with metallic cores are biocompatible within the experimental time period (4 h in cultures and 7 days in whole animals). CeO_2 nanoparticles induced an increase in luciferase signal/photon intensity comparable to the control, saline injection, while CdTe non-PEGylated particles produced the most robust astrocyte activation. (Figure 3). We suggest that CdTe QDs and CeO_2 nanoparticles could serve as positive and negative controls (in addition to saline) in the testing of other nanoparticles in this and similar animal models to assess activation of glia in real time.

PEG is widely accepted as a suitable biopolymer for preclinical biological experiments and some biomedical applications. PEG chain length is essential for nanoparticle stability, dispersion in aqueous media, and protection of the core.[32,33] PEGylated nanoparticles such as micelles and liposomes are excellent drug carriers for lipophilic agents (e.g., sex hormones,[34] fluorescent dyes, or radiolabeled agents), and certain PEGs were even beneficial in animals following acute spinal cord injuries.

Most of the presently available QDs are PEGylated but without specific ligands. Such particles are internalized to a different extent in various cells, but neurons take up only a few. Neuron-specific internalization can be achieved by corona modification with neuron-specific ligands. Few second- and third-generation QDs are currently investigated in several laboratories.[35−38] However, real-time imaging in live mice in conjunction with functional response to nanoparticles in the CNS (e.g., glial activation) were not previously reported. The approach described here is widely applicable for testing the responsiveness of neural and glial cells to other nanomaterials in the nervous system and other tissues.

Dual labeling of organelles and QDs used in this study provided a clear evidence for colocalization of these nanoparticles and lysosomes but not mitochondria (Figure 5). Both glial cells and neurons appeared normal, and there was no significant loss of cells or marked morphological change suggestive of degenerative processes within the imaging period (4 h). PEGylated QD 565 and QD 655 were biocompatible with human keratinocytes, whereas negatively charged ones were toxic.[16] Our results obtained with cerium

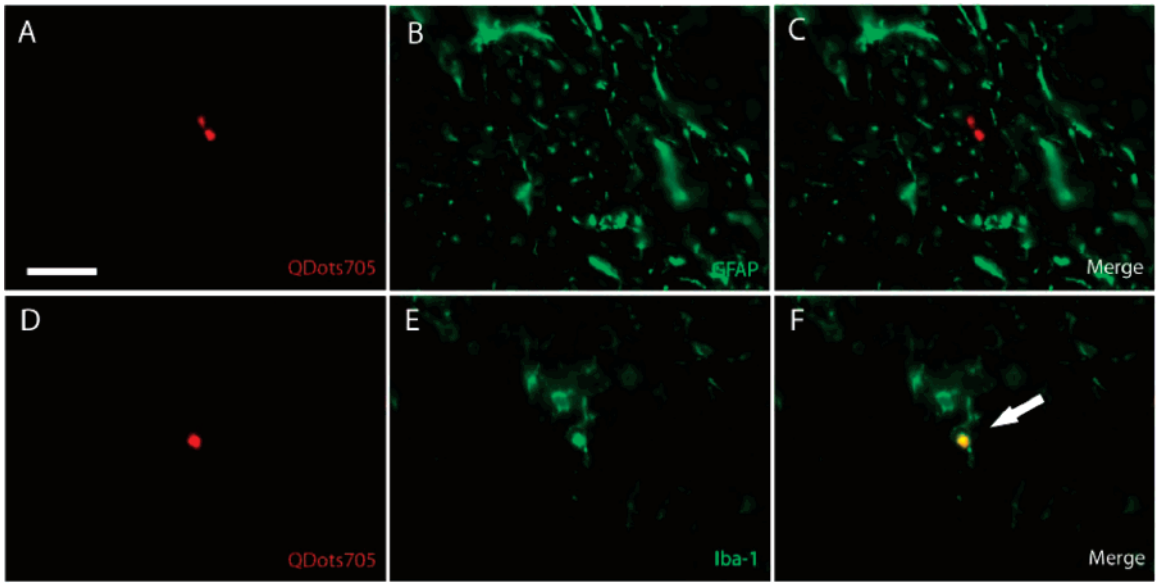

Figure 4. Localization of intracortically administered nanoparticles reveals colocalization with Iba-1 positive cells. (A) QD 705, (B) activated astrocyte surrounding the site of injection (anti-mouse GFAP 1:1000), (C) overlay. (D) QD 705, (E) Iba-1 positive microglial cells displaying amoeboid activated morphology (antirat polyclonal Iba-1, 1:1000), (F) colocalization between QD and Iba-1 positive cell (arrow). Scale bar = 25 μm.

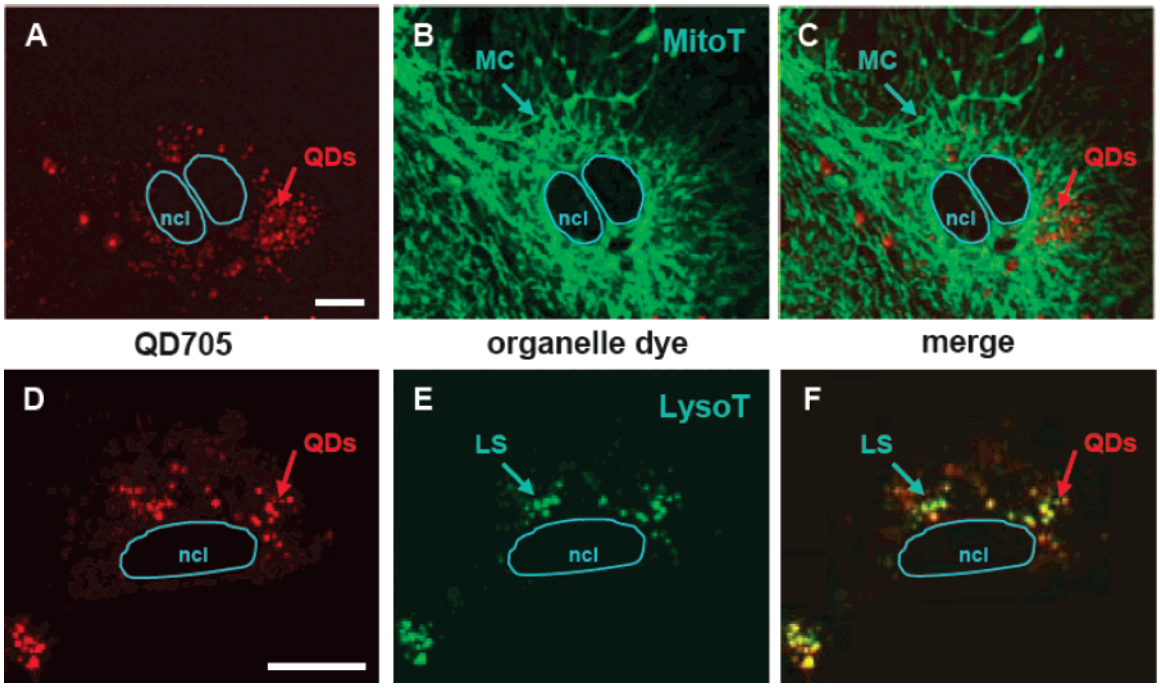

Figure 5. Subcellular localization of QD 705 in primary neural (cortical) cultures. (A) QD 705 (30 nM; 4 h treatment); (B) MitoTracker deep red (1 μM); (C) overlay (A and B); (D) QD 705; (E) LysoTracker green DND 26 (0.5 μM); and (F) colocalization between the QD and lysosomes. Scale bar = 10 μm.

nanoparticles confirm previous findings that these are non-deleterious under the employed experimental conditions.

In summary, results from these studies show that: (i) QDs 705 have excellent photophysical properties for repeated real-time imaging without causing marked tissue damage, (ii) the strong photoluminescence of QDs 705 makes them a suitable imaging tool to study their subcellular localization and fate in live animals and in primary neural cultures, and (iii) the imaging approach presented here utilizes transgenic animals with astrocyte-responsive reporter (luciferase) together with highly luminescent QDs. This approach may be widely applicable for assessing nanoparticle-induced tissue response in live animals in real time.

Acknowledgment. We acknowledge partial financial support from Canadian Institutes of Health Research (CIHR) and Natural Sciences and Engineering Research Council (NSERC). J.K. is recipient of the Career Award from the R&D Health Research Foundation and CIHR. M.L.-H. is recipient of the CIHR Canada Doctoral Scholarships.

Supporting Information Available: Experimental details including reagents, cell culture, cell staining, preparation and accessibility of nanoparticles, flow cytometric analysis (FACS), confocal microscopy, and in vivo optical small animal imaging as well as supplementary figures. This material is available free of charge via the Internet at http://pubs.acs.org.

References

(1) Nishiyama, N.; Kataoka, K. *Pharmacol. Ther.* **2006**, *112* , 630−648.
(2) Giepmans, B. N.; Adams, S. R.; Ellisman, M. H.; Tsien, R. Y. *Science* **2006**, *312*, 217−224.
(3) Maysinger, D.; Lovric, J.; Eisenberg, A.; Savic, R. *Eur. J. Pharm. Biopharm.* **2007**, *65*, 270−281.
(4) Duncan, R. *Nat. Rev. Cancer* **2006**, *6*, 688−701.
(5) Savic, R.; Luo, L.; Eisenberg, A.; Maysinger, D. *Science* **2003**, *300*, 615−618.
(6) Savic, R.; Azzam, T.; Eisenberg, A.; Maysinger, D. *Langmuir* **2006**, *22*, 3570−3578.
(7) Medintz, I. L.; Uyeda, H. T.; Goldman, E. R.; Mattoussi, H. *Nat. Mater.* **2005**, *4*, 435−446.
(8) Alivisatos, A. P.; Gu, W.; Larabell, C. *Annu. Rev. Biomed. Eng.* **2005**, *7*, 55−76.
(9) Nel, A.; Xia, T.; Madler, L.; Li, N. *Science* **2006**, *311*, 622−627.
(10) Cho, S. J.; Maysinger, D.; Jain, M.; Roder, B.; Hackbarth, S.; Winnik, F. M. *Langmuir* **2007**, *23*, 1974−1980.
(11) Xia, T.; Kovochich, M.; Brant, J.; Hotze, M.; Sempf, J.; Oberley, T.; Sioutas, C.; Yeh, J. I.; Wiesner, M. R.; Nel, A. E. *Nano Lett.* **2006**, *6*, 1794−1807.
(12) Zanello, L. P.; Zhao, B.; Hu, H.; Haddon, R. C. *Nano Lett.* **2006**, *6*, 562−567.
(13) Ryman-Rasmussen, J. P.; Riviere, J. E.; Monteiro-Riviere, N. A. *Nano Lett.* **2007**, *7*, 1344−1348.
(14) Seleverstov, O.; Zabirnyk, O.; Zscharnack, M.; Bulavina, L.; Nowicki, M.; Heinrich, J. M.; Yezhelyev, M.; Emmrich, F.; O'Regan, R.; Bader, A. *Nano Lett.* **2006**, *6*, 2826−2832.
(15) Cambi, A.; Lidke, D. S.; Arndt-Jovin, D. J.; Figdor, C. G.; Jovin, T. M. *Nano Lett.* **2007**, *7*, 970−977.
(16) Ryman-Rasmussen, J. P.; Riviere, J. E.; Monteiro-Riviere, N. A. *J. Invest. Dermatol.* **2007**, *127*, 143−153.
(17) Ballou, B.; Ernst, L. A.; Andreko, S.; Harper, T.; Fitzpatrick, J. A.; Waggoner, A. S.; Bruchez, M. P. *Bioconjugate Chem.* **2007**, *18*, 389−396.
(18) Bentzen, E. L.; Tomlinson, I. D.; Mason, J.; Gresch, P.; Warnement, M. R.; Wright, D.; Sanders-Bush, E.; Blakely, R.; Rosenthal, S. J. *Bioconjugate Chem.* **2005**, *16*, 1488−1494.
(19) Boulmedais, F.; Bauchat, P.; Brienne, M. J.; Arnal, I.; Artzner, F.; Gacoin, T.; Dahan, M.; Marchi-Artzner, V. *Langmuir* **2006**, *22*, 9797−9803.
(20) Yu, W. W.; Chang, E.; Drezek, R.; Colvin, V. L. *Biochem. Biophys. Res. Commun.* **2006**, *348*, 781−786.
(21) Gao, X.; Cui, Y.; Levenson, R. M.; Chung, L. W.; Nie, S. *Nat. Biotechnol.* **2004**, *22*, 969−976.
(22) Fischer, H. C.; Liu, L.; Pang, K. S.; Chan, W. C. W. *Adv. Funct. Mater.* **2006**, *16*, 1299−1305.
(23) So, M. K.; Xu, C.; Loening, A. M.; Gambhir, S. S.; Rao, J. *Nat. Biotechnol.* **2006**, *24*, 339−343.
(24) Kim, S.; Lim, Y. T.; Soltesz, E. G.; De Grand, A. M.; Lee, J.; Nakayama, A.; Parker, J. A.; Mihaljevic, T.; Laurence, R. G.; Dor, D. M.; Cohn, L. H.; Bawendi, M. G.; Frangioni, J. V. *Nat. Biotechnol.* **2004**, *22*, 93−97.
(25) Frangioni, J. V.; Kim, S. W.; Ohnishi, S.; Kim, S.; Bawendi, M. G. *Methods Mol. Biol.* **2007**, *374*, 147−160.
(26) Ridet, J. L.; Malhotra, S. K.; Privat, A.; Gage, F. H. *Trends Neurosci.* **1997**, *20*, 570−577.
(27) Pekny, M.; Nilsson, M. *Glia* **2005**, *50*, 427−434.
(28) Zhu, L.; Ramboz, S.; Hewitt, D.; Boring, L.; Grass, D. S.; Purchio, A. F. *Neurosci. Lett.* **2004**, *367*, 210−212.
(29) Kadurugamuwa, J. L.; Modi, K.; Coquoz, O.; Rice, B.; Smith, S.; Contag, P. R.; Purchio, T. *Infect. Immun.* **2005**, *73*, 7836−7843.
(30) Qi, X.; Lewin, A. S.; Sun, L.; Hauswirth, W. W.; Guy, J. *Invest. Ophthalmol. Vision Sci.* **2007**, *48*, 681−691.
(31) Lovric, J.; Cho, S. J.; Winnik, F. M.; Maysinger, D. *Chem. Biol.* **2005**, *12*, 1227−1234.
(32) Tessmar, J. K.; Gopferich, A. M. *Macromol. Biosci.* **2007**, *7*, 23−39.
(33) Torchilin, V. P. *Pharm. Res.* **2007**, *24*, 1−16.
(34) Lim Soo, P.; Lovric, J.; Davidson, P.; Maysinger, D.; Eisenberg, A. *Mol. Pharm.* **2005**, *2*, 519−527.
(35) Le Gac, S.; Vermes, I.; van den Berg, A. *Nano Lett.* **2006**, *6*, 1863−1869.
(36) Silva, G. A. *Nat. Rev. Neurosci.* **2006**, *7*, 65−74.
(37) Pathak, S.; Cao, E.; Davidson, M. C.; Jin, S.; Silva, G. A. *J. Neurosci.* **2006**, *26*, 1893−1895.
(38) Sundara Rajan, S.; Vu, T. Q. *Nano Lett.* **2006**, *6*, 2049−2059.

NL071611T